Anisotropic distortion and Lifshitz transition in α-Hf under pressure

Weiwei Sun,[1,2] Wei Luo,[1,*] Qingguo Feng,[3,4] and Rajeev Ahuja[1,2]

[1]*Department of Physics and Astronomy, Uppsala University, Box 516, SE-75120 Uppsala, Sweden*

[2]*Department of Material Science and Engineering, KTH-Royal Institute of Technology, SE-10044 Stockholm, Sweden*

[3]*Department of Physics, Chemistry and Biology, Linköping University, SE-58183 Linköping, Sweden*

[4]*Swedish e-Science Research Centre (SeRC), Linköping University, SE-58183 Linköping, Sweden*

(Received 24 October 2015; revised manuscript received 27 January 2017; published 14 March 2017)

In this work we report a theoretical investigation on behavior of the elastic constant C_{44} and the transverse optical phonon mode E_{2g} of α-Hf under pressure within the density functional theory. In contrast to many other reported transition metals, the above two quantities do not show a synchronous relation as pressure increases. Below 13 GPa, an opposite shifting tendency has been observed. However, once the pressure is raised above 13 GPa, the trend is pulled back to be consistent. This anomalous behavior is figured out to be caused by the large lattice anisotropy of the c/a ratio along with the elastic anisotropy. The synchronous behavior is found to be in accordance with the behavior of c/a ratio with increased pressure. In our band-structure investigations the electronic topological transition has been discovered at 10 GPa, which relates to the change of c/a ratio suggested by recent literature. The presence of the Van Hove singularity shown in the densities of states has been identified and regarded as the origin of the variation of C_{44} and E_{2g}.

DOI: 10.1103/PhysRevB.95.115130

I. INTRODUCTION

The Group-IV elements Ti, Zr, Hf and their alloys have drawn great scientific and industrial interests due to their characteristic applications in aerospace, nuclear reactors, and the chemical industry due to their mechanical strength, stiffness, resistance to degradation in elevated temperature, light weight, and corrosion resistance [1]. Particularly, Hf has been widely used in reactor-control rods due to its good absorption cross-section for thermal neutrons and excellent mechanical and corrosion-resistant properties. Moreover, Hf also exhibits many other peculiar properties, such as high melting point, high hardness, and superconductivity [2–5]. Many of these phenomena are associated with the vibrational and elastic properties, so that it is of much significance and in vigorous demand to investigate the properties under pressure such as the structural stability and phase transitions. As other Group-IV transition-metal (TM) elements, at ambient conditions, Hf crystallizes into a hexagonal closed-packed (hcp) structure (α phase, two atoms per unit cell with D3h symmetry). As pressures increases above the critical value, it transforms to the ω phase (hexagonal, three atoms per unit cell) [6].

In a hexagonal lattice, at the Γ point, the three acoustic modes are presented by $A_{2u} + E_{1u}$, and the lowest optical mode is a Raman-active mode, E_{2g}. Verified by several studies [7,8], this E_{2g} is closely connected to the elastic constant C_{44} by the following relation:

$$\nu(E_{2g}) = \frac{1}{2\pi}\sqrt{\frac{4\sqrt{3}a^2C_{44}}{mc}}, \tag{1}$$

where a and c are the lattice constants, and m is the atomic mass. Equation (1) reveals that the square root of C_{44} is proportional to E_{2g} when under compression. This is the foremost and encouraging point that a reasonable estimation of C_{44} can be carried out directly from the experimental measurement of the E_{2g} phonon mode, with regard to the fact that direct experimental measurement of C_{44} is quite difficult at high pressure. Although the recently developed inelastic x-ray scattering method has emerged and has been used to study the elastic moduli of transition metals Co [9], Fe [10], and MgO [11]. Reaching the hydrostatic condition is still considered as an obstacle and needs further efforts. Actually, the values of C_{44} for a large number of hexagonal TMs have been estimated by using Eq. (1), and excellent agreement with those experimental results has been identified [7,8,12]. In this scenario, this method paves the way to investigate the structural and vibrational properties of TMs.

As for these two quantities, in the harmonic model the elastic constant C_{44} is dependent on the relative lateral motion of the undeformed basal planes, and this motion is also the determinant of the E_{2g} mode. The combination of the central and angular forces between the sets of neighbors (involving two adjacent basal planes) reveals a relation between the elastic constant C_{44} and the E_{2g} mode. If the nature of the two quantities is traced back, the E_{2g} Raman tensor can be written as

$$\begin{pmatrix} d & \cdot & \cdot \\ \cdot & -d & \cdot \\ \cdot & \cdot & \cdot \end{pmatrix},$$

where d represents the displacement and there are two opposite displacements for the two atoms. To determine the C_{44}, a strain matrix ε is applied to the unity. For a hexagonal lattice, to determine C_{44} we use a monoclinic strain of space group C2/m represented by

$$\varepsilon = \begin{pmatrix} 0 & 0 & \delta \\ 0 & \delta^2/(1-\delta^2) & 0 \\ \delta & 0 & 0 \end{pmatrix},$$

where δ is the magnitude of the applied strain, and it can be implied that the C_{44} partially accounts for the in-plane response of distortion. The two representations above validate Eq. (1),

*wei.luo@physics.uu.se

 ©2017 American Physical Society

showing that both C_{44} and E_{2g} serve as the response of the in-plane perturbation. So far, the relation of C_{44} and E_{2g} under pressure in many hexagonal TMs has been inspected, and most of the elements satisfy Eq. (1). For Group IV elements, only Ti and Zr have been studied and examined by Eq. (1). It was reported that the C_{44} values calculated in Eq. (1) from the E_{2g} mode increase as pressure increases, and the measured C_{44} coincides with the calculated one estimated via Eq. (1) [13], while information for Hf is missing. It has been unveiled that the transition pressure of Ti (ranging from 2.9 to 11 GPa) [14] and Zr ($\sim$2.2 GPa) [15] to the ω phase are very different from Hf. Several experimental and theoretical studies have shown that the α to ω phase transition of Hf occurs around 40 GPa [6,16–18]. In fact, the E_{2g} optical phonon mode and the coupled elastic shear modulus C_{44} were experimentally found to show an anomalous pressure-dependent behavior [19], but up to now this issue has not been clarified yet. It was also reported that the lattice distortion will shift the degeneracy of the bands in the A-H-L plane, and for the bands close to the Fermi level this splitting will reduce the electronic energy and a phonon anomaly will occur [20]. Despite the anomalous behavior mentioned in the studies above, no clear theoretical clues have been provided, i.e., the relation between mechanism and phenomena is still not established. To investigate the anomaly in α Hf and its origin, we performed this theoretical study.

Based on the above reasons and ambiguities, between ambient conditions and 40 GPa, C_{44} and E_{2g}, along with the electronic band structures and density of states (DOS), were calculated and examined for α Hf. The unique pressure-dependent vibrational and elastic properties in α Hf are confirmed and found to be associated with the electronic topological transition (ETT), also known as the Lifshitz transition [21]. The behavior of C_{44} and E_{2g} of α Hf under pressure shows that, below 13 GPa they are not synchronous but become consistent in changing at higher pressure. This anomaly is attributed to be the consequence of the large anisotropic effects of the lattice induced by the electronic topological changes of the electronic bands. The E_{2g} mode also responds to the occurrence of ETT under pressure, and this behavior can be also detected for C_{44} and the c/a ratio.

II. COMPUTATIONAL METHODS

In this work density functional theory (DFT) calculations were carried out with the Vienna *Ab-Initio* Simulation Package (VASP) [22,23] and the full-potential local-orbital code (FPLO9.01.35) [24]. Spin-orbit coupling was taken into account in all calculations due to the presence of the heavy element Hf. For TM atoms, spin-orbit coupling largely determines the multiple structures and, in solids, the band structures are mainly controlled by spin-orbit coupling along with crystal-field splitting [25]. Note that the role and necessity of relativistic calculations have been discussed (based on band-structure calculations) and included in the supplementary information (SI) [26].

The structural optimization, the calculations of elastic constants (stress-strain method [27,28]) and phonon frequencies [both the frozen phonon approach [29] and density functional perturbation theory (DFPT)] were performed within VASP. The projected-augmented wave (PAW) [30] method was used with the generalized gradient approximation (GGA) in the Perdew, Burke, and Ernzerhof (PBE) functional [31]. For better convergence of the physical quantities, a dense mesh with $39 \times 39 \times 33$ k points was used, which is much denser than that in previous work [17]. For Brillouin-zone (BZ) integration the first order of the Methfessel–Paxton method [32] was applied with a width of 0.05 eV, in which the maximum entropy value of 1 meV per atom has been achieved. Moreover, a relaxation convergence of 0.01 eV for ionic positions, an electronic convergence of 0.001 meV, and a cutoff energy of 600 eV were employed throughout the calculations. During the relaxations, a specific pressure as a target is approached self-consistently, and the lattice parameters are obtained as the results. It is found that this pressure-volume curve only shows slight difference in comparison with the one fit by the third-order Birch–Murnaghan equation of states [33–35]. The comparison between the two pressure-volume curves is hence plotted and reported in the SI [26]. The phonon spectra has been computed by employing the PHONOPY code [36]. In the phonon calculations, a $3 \times 3 \times 2$ supercell was constructed to ensure the convergence of the forces. We have also checked the convergence in term of supercell size. The full-potential local-orbital (FPLO) code has been used to calculate the electronic structure extensively based on the relaxed structures from VASP due to that in FPLO, an accurate and complete description of both core and valence electrons can be realized. Within FPLO, the PBE functional was adopted as the exchange correlation functional in the GGA within the four-component fully relativistic framework, and a expanded valence basis set with $4s$, $4p$, $5s$, $6s$, $4d$, $5d$, $5p$ states has been used for Hf. All the band-structure calculations were carefully converged with respect to the k-point mesh and $40 \times 40 \times 40$ points, and a rather denser k mesh with $45 \times 45 \times 45$ points was used to compute the DOS.

III. RESULTS

A. Structural, elastic, and vibrational properties

To check the dynamical stability of α Hf, the phonon dispersion curves (PDCs) from 0 to 40 GPa are calculated for α Hf and plotted in Fig. 1. Within this pressure range, the frequencies of all phonon modes are positive, indicating that, up to 40 GPa, α Hf is dynamically stable. This coincides with previous experimental and theoretical findings [6,16,17]. Moreover, the simulated spectra is in good agreement with the experimental data, as shown by pink stars in Fig. 1. It can also be noticed that, along the A-K-M path, the optical phonon modes are shifted upward with increasing pressure but decrease at the Γ point. These distinctive tendencies can be related to the behavior in an anisotropic hexagonal lattice.

Followed by the phonon spectra, the behavior of the C_{44} and E_{2g} modes are plotted in Fig. 2. Basically, C_{44} rises from 0 GPa until 17 Gpa, and then falls into a steady decease above 17 GPa. The increase of C_{44} in the low-pressure range suggests that the pressure is hardening the basel plane, while above 17 GPa it is weakened by compression. Concerning the E_{2g} mode, we can distinguish the disparities by different means of calculating this quantity (in red and blue), whereas, in an

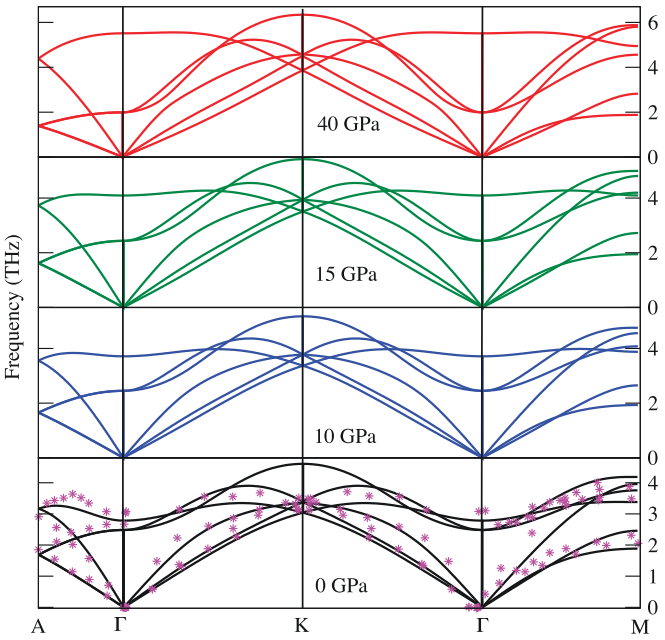

FIG. 1. The phonon dispersion curves for α-Hf under pressure from 0 GPa (black curves), 10 GPa (blue curves), 15 GPa (green curves), to 40 GPa (red curves) respectively. The pink stars present the experimental data measured by neutron spectroscopy at 295 K [20].The red arrow points out the E_{2g} mode in the phonon spectra.

overview, the E_{2g} mode is softened in the investigated pressure range. Particularly for the curve of the single-q method (in blue), a local minima-maxima feature appears in the regime between 13 and 17 GPa, and then a decrease of the E_{2g} mode is observed, which is in a good agreement with the behavior of C_{44}. As the C_{44} curve (in black) shown in Fig. 2, below 17 GPa

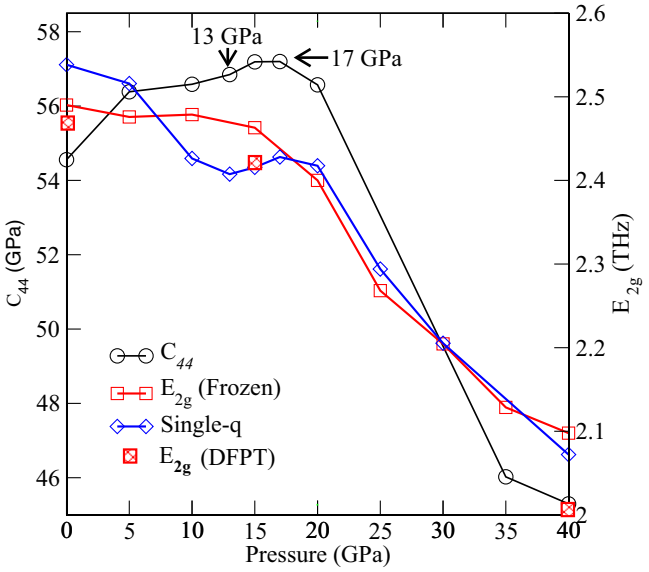

FIG. 2. The shift of C_{44} and E_{2g} as a function of pressure. The circles denote the C_{44} and the squares denote the E_{2g}. The hollow squares present E_{2g} calculated with the frozen phonon (Frozen) method while the filled ones are obtained with DFPT. The blue curves presenting E_{2g} are obtained by the single-q method.

it continues to rise and then reaches a maxima at 17 GPa. These results lead to the conclusion that, when below 13 GPa, no synchronous relation between E_{2g} and C_{44} is present, which contradicts the results of many reported examples of hexagonal TMs [12], while above 13 GPa, C_{44} and E_{2g} return to the same track. The anomalous inconsistency with the C_{44} curve emerges from 0 GPa but terminates at 13 GPa, demonstrating that the behavior of α Hf does not fully satisfy Eq. (1).

Then the origin of the shown deviations found in the three methods is discussed below. Within the frozen phonon approach, the dispersion relation is obtained at certain number of $\boldsymbol{k}$-points through Fourier interpolation or similar schemes, which implies that numerical errors may probably have been included. The DFPT method is based on the response to arbitrary (infinitesimal) displacements of the atoms and to corresponding changes of the ionic potential by perturbation theory. The shift of the E_{2g} mode is evaluated in the DFPT method at selected pressures (0, 15, and 40 GPa) presented by the filled squares in Fig. 2. The tendency of E_{2g} under pressure from the DFPT method coincides with that from the frozen phonon approach. The distinctive issue is that the values of the E_{2g} mode calculated in DFPT is lower than those obtained by frozen phonon method. This can be explained by noting that, in DFPT, the Fourier transform of the force constant can be calculated from the linear response $\partial n(r)/\partial u_s^{\alpha}(q)$ and then diagonalized to acquire the phonon modes at q. It is noticeable that $n(r)$ is the average electron density so that it has only a marginal effect on E_{2g}.

Instead of inspecting the full phonon spectra, one can concentrate only on the single-q point; Γ in this case. It is noticeable that the E_{2g} mode calculated by the single-q point method (see blue curve in Fig. 2) are determined by the Hessian matrix (matrix of second derivatives of energy with respect to atomic displacements). The zone-center phonon frequencies computed by these means are more precise than those calculated from the frozen phonon method or the perturbation method in a finite-size supercell. It is clear that the three methods provide a similar E_{2g}-pressure (P) relation that the compression will suppress this phonon mode.

Now questions arise as follows: What is the origin of this anomalous behavior in α Hf? Why is the conclusion for α Hf not in a line with TM elements satisfying Eq. (1) [12]? As we have observed that, for α Hf, the behavior of the C_{44} and E_{2g} modes under pressure is not synchronous below 13 GPa, which does not fulfill Eq. (1). In fact, Zn, Cd, and Tl are the exceptions that do not obey the rule of Eq. (1) [12]. Although there is no direct theoretical link with lattice anisotropy, all the above-mentioned metals exhibit very large lattice anisotropies [37]. For Zn and Cd, the distances between one atom and its out-of-plane neighbors are different from those in the basal plane and their linear differences in compressibility are considerably large [38]. This manifests that they possess high elastic anisotropy, and this anisotropic effect is likely to be the origin of the mismatch between C_{44} and E_{2g} in Zn, Cd, Tl as well as Hf in this study.

Before heading to the lattice anisotropy, we can evaluate the elastic anisotropy, which is a macro property related to the lattice anisotropy. As is known, for an elastically isotropic hexagonal crystal, the three anisotropy ratios must be simultaneously equal to unity [39], where the three anisotropic

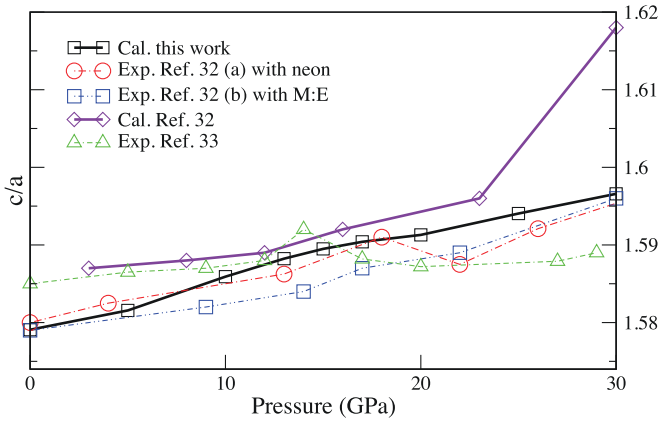

FIG. 3. In the upper panel, the behavior of the lattice parameters c/a as a function of pressure is plotted. The solid curves are the theoretical results, where the violet curve is extracted from Ref. [32], and the black curve is obtained in this work. The dashed lines with dots are experimental results, where the red and blue curves are two measurements extracted from Ref. [33]. The green curve is from Ref. [34]. In the lower panel, the curvature of $\ln(a)$ in black, $\ln(c)$ in red, and $\ln(c/a)$ in blue with respect to the pressure (P) are depicted to monitor the lattice anisotropy.

constants are presented by

$$A_1 = 2C_{44}/(C_{11} - C_{12}), \quad A_2 = C_{33}/C_{11}, \quad A_3 = C_{12}/C_{13}. \tag{2}$$

At ambient conditions, the anisotropic constants of α Hf are 0.97, 1.07, and 1.03 for A_1, A_2, and A_3, respectively. However, A_2 rises to 1.12 when A_3 and A_1 decrease dramatically during compression. The computed large deviation in anisotropic constants from unity reveals that α Hf has a large anisotropic distortion under pressure. Having these anisotropic constants obtained from elastic constants, we are about to address the lattice behavior under pressure followed by the finding of anomalous behavior of E_{2g} and C_{44}. Note that the pressure-dependent elastic moduli can be found in the SI [26].

Since the lattice parameters are in a close relation with the elastic constants, particularly for a hcp lattice, the evolution of c/a with pressure is hence illustrated in Fig. 3 up to 30 GPa as the anomalous behavior is observed below 20 GPa. In the upper panel, the black curve in Fig. 3 shows an increasing tendency with a smoothing bump around 15 GPa. This phenomenon illustrates that a lattice distortion is present and becomes highly anisotropic with the stronger compression. Our calculated result is consistent with another simulation shown as the purple line, and it also follows the measured relation in experiments shown as the blue curve. All the shown experimental results (in red, blue, and green) exhibit an increasing tendency in this pressure regime, but there are indeed differences lying on the occurrence of a local maxima or bump as well as a changing tendency above it. In the two measurements (red and green curves), local maxima have been observed, while another experimental measurement (in blue) shows a similar changing trend in this work (in black).

To further characterize the anisotropy, the curvatures of $\ln(a)$, $\ln(c)$, and $\ln(c/a)$ as a function of pressure are plotted in the lower panel of Fig. 3. The quantities can serve a better role in monitoring the pressure effects on in-plane, out-of-plane directions of the lattice, and the lattice anisotropy, respectively. With increasing compression, both the c and a parameters decrease. The derivative $d\ln(a)/dP$ experiences a rapid increase up to 17 GPa, and then a mild increase above that pressure. As for $d\ln(c)/dP$, the increase starts slowing from 10 GPa and afterwards a linear relation is present above 17 GPa. These results reveal that the lattice parameter a is suppressed more than c, and both c and a have gone through a moderate change at 17 GPa. In addition, the $d\ln(c/a)/dP$ curve illustrates that the pressure reverses the rising tendency of the c/a ratio so that it decreases above 10 GPa. It is believed that the lattice is becoming more anisotropic with increasing compression, and the variation of lattice parameters all show anomalous changes at 17 GPa. This coincides with the starting point of the consistent softening of C_{44} and E_{2g} shown in Fig. 2.

As a matter of fact, the anomalous phenomena with compression that occurs for c/a is also present in Fe [40], Co [41], Zn [42], and Os [43], which as reported results from ETT. According to the above discussions, a perturbation on $d\ln(c/a)/dP$ appears at 10 GPa, and a drastic change takes place at 17 GPa in α Hf. It is emphasized that, for Co, not only the anomaly in c/a but also the elastic moduli are found to be altered by ETT. Coincidentally, in our investigated pressure regime, the C_{44} and E_{2g} curves versus pressure do exhibit dissimilar trends. In addition to the possible influence of ETT, it was also reported that the anisotropy is caused by the asymmetric charge distribution of the d electrons in these metals [44]. Generally, transition metals have a relatively narrow d band in the middle of a broad sp band, which has an impact on its electronic and superconductive properties. The electronic transfer between the broad sp band and the narrow d band is the driving force behind the transition in electronic structure as well as the phase transition partially [14,45–48].

B. Electronic properties

The electronic structure calculations are now performed, and the band structure together with total DOS in a relative narrow regime from −0.6 eV until 0.6 eV are reported in Fig. 4. The drastic changes of bands along A-H-L under pressure enormously attract our attention. It can be found that a quasiconcave band beneath E_F and another deeper quasiflat band are located at the H high-symmetry point. At 10 GPa, the pressure lifts up the quasiconcave band to E_F at the H point, and this i a definite sign of ETT induced by pressure. Note that the A-H point lies in the basal plane. As further compression imposes, this quasiconcave band moves upward smoothly, and until 40 GPa, the quasiconcave band completely resides above E_F. In this process, in the left wing of the A-H path, the quasiconvex band is gradually bent. Another interesting phenomenon is that a band splitting highlighted by the red ellipsoids takes place at 30 GPa, which indicates that lowering symmetry occurs by imposing pressure. More importantly, this symmetry breaking can only be present when a fully relativistic calculation is performed, as shown in the SI [26].

Turning our concentration to the Γ-A path, the electron pocket is diminishing with elevated pressure, which is likely to induce another ETT above 40 GPa. One should bear in mind

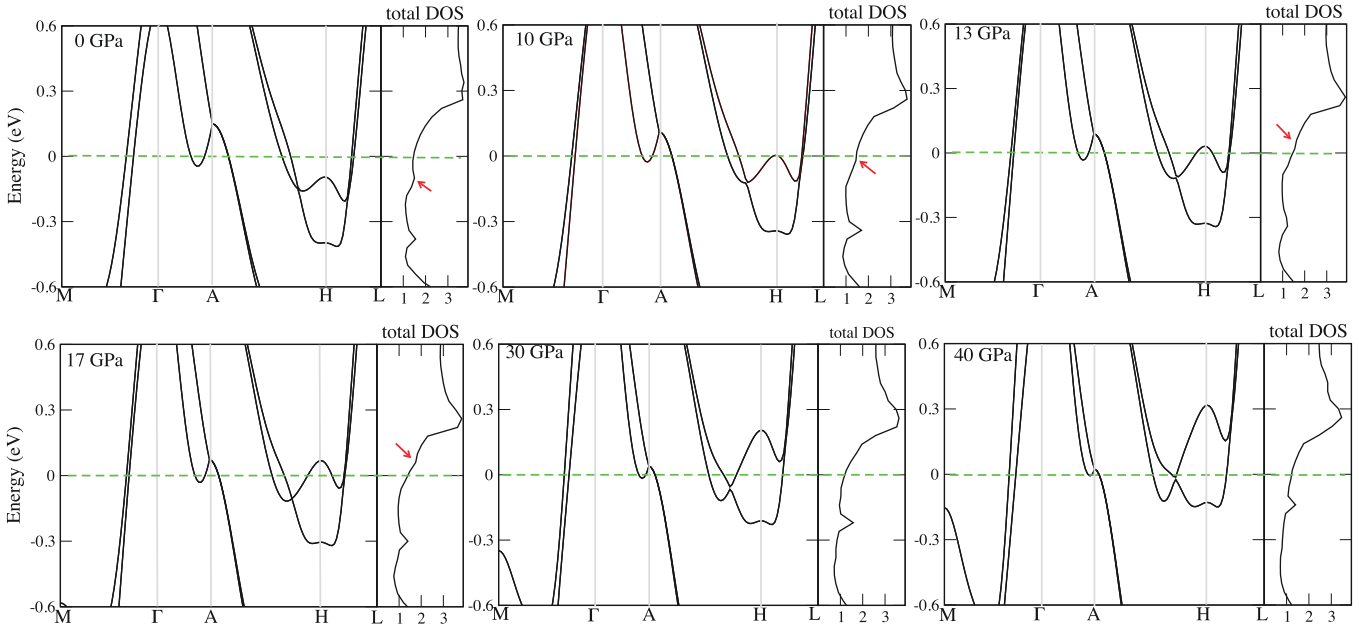

FIG. 4. The band structure of Hf with varied pressures of 0, 5, 10, 13, 17, 30, and 40 GPa. The red ellipsoids highlight the evolution of the bands showing drastic changes. On the right side of each band structure, the total density of states is also present. The red arrows highlight the position of the singularity. The Fermi level is set to 0 eV as the green dashed line indicates.

that the α phase is stable up to 40 GPa, so that our study will not step out of this regime. Further moving to the M-Γ path, up to 40 GPa, no ETT can be observed, but a band is rising towards to E_f (see bands at 30 and 40 GPa) and will likely pass E_f when above 40 GPa. This implies that ETTs may be the driving force of the phase transition from the α to the ω phase. Moreover, ETT occurs in the A-H-L path, manifesting its anisotropic feature since no anomalous phenomenon has been found out of plane yet.

On the right side of the bands, we concentrate on the total DOS shown in Fig. 4. It can be found that there is an obvious kink located at -0.1 eV at ambient conditions (as the red arrow points out). With the increase of pressure, it moves towards the higher binding energy. At 10 GPa, the kink is placed at E_f, which is in accordance with the occurrence of the ETT at the H point as the bands indicate. Usually the electronic structural transition can be reflected by a so-called Van Hove singularity [49], which is shown as a kink in DOS referring to extrema or saddle points at critical points in the BZ. Combining with the evolution of the bands, the appearance of a Van Hove singularity both clearly leads to an ETT.

IV. DISCUSSIONS

In most alkaline and transition metals or even rare-earth elements, the valence d electrons are rather localized and are closer to the nucleus than s electrons [50]. Thus, the compression raises the energy of the s state and enables electron transfer to d states, which changes the crystal structure [51,52]. The behavior of s-d transfer is thus interesting to be studied. Additionally, whether the unusual phenomenon can occur in electron transfer or not is another mystery. Carrying these questions, we step further into the pressure-dependent s-d transfer behavior shown in Fig. 5(a) and the number of states at E_f, i.e., $\rho(E_f)$ shown in Fig. 5(b). The 6s and 5d projected DOS are also given in Figs. 5(c) and 5(d), respectively. The orbital transformation rate can be presented by

$$\frac{N_L(P) - N_L(0)}{N_L(0)},$$

where $N_L(P)$ is the occupancy of the orbital with orbital index L, e.g., the 6s orbital, at a specific pressure P. In Fig. 5(a), the s-d transfer occurs in Hf as other transition metals do, so that this indicates that α Hf is a typical transition metal, where the transformation rate for 6s monotonically decreases while that of 5d monotonically increases without any maxima or minima. Concerning the states at E_f, Fig. 4 shows the singularity, and its motion implies that the pressure-induced ETT alters the electronic structure at E_f. In Fig. 5(b), $\rho(E_f)$ at 10 GPa hits a peak, which is in accordance with the findings from Fig. 4.

Despite the ETT occurs at 10 GPa, no sign of anomaly is observed on the orbital transformation rate between 6s and 5d orbitals as shown in Fig. 5(a). For the sake of digging, we have taken out the 6s and 5d projected DOS for further discussion. Under pressure, band broadening has been found in both 6s and 5d orbitals. In Fig. 5(c), one can see that the 6s states are initially dominant at -3.8 eV, and then are broadening occurs with rising pressure. To the right side of this broad peak, a tail-like structure prevails toward E_f. On both sides of E_f, two small humps are present respectively at -1 and 1 eV. Combining with 5d in Fig. 5(d), a strong s-d hybridization is observed around -1 eV, which provides a tunnel for s-d electron transfer. In Fig. 5(d), the 5d states dominate mainly between -2 and 2 eV with E_f residing in a broad valley between the two enhanced peaks at ± 1 eV. Inside this broad valley, a sharp peak appears initially with a small hump at the edge of the strong right peak, showing as the above-reported singularity. This sharp peak is either enhanced

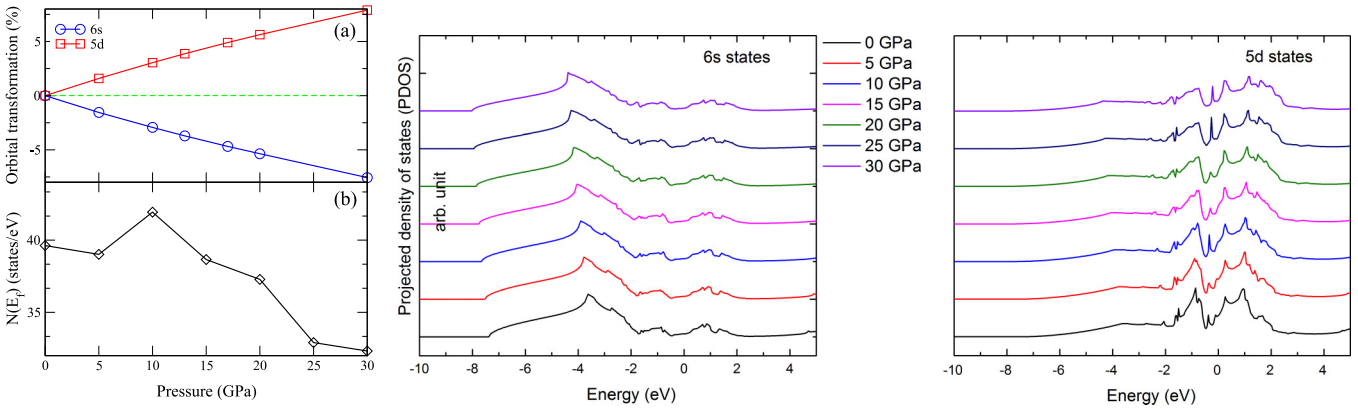

FIG. 5. (a) 6s (blue) and 5d (red) orbitals transformation rate under pressure. (b) The number of states at the Fermi level, $\rho(E_f)$ as a function of pressure. (c) Evolution of the DOS of 6s and (d) DOS of 5d orbital with pressure.

or weakened under various pressure, but clearly stays below E_f. But the hump is suppressed and finally disappears. From the plotted DOS, the singularity mainly relates to the 5d states. The evolution of this singularity addresses the ETT and then can connect to other anomalous phenomena.

In fact, the relation between ETT and C_{44} is bounded to $\rho(E_f)$, and the observed anomalous behavior in the DOS shown in Fig. 4 can be better interpreted in Fig. 5(b). In the one-electron approximation, the shift of the elastic constant C_{ij} is connected to DOS(E_f) by the following equation [53]:

$$C_{ij} \propto \left.\frac{d\rho(E)}{dE}\right|_{E=E_f}, \tag{3}$$

which illustrates that the elastic moduli will be intensively perturbed when a drastic change occurs in the curvature of $\rho(E_f)$. When the ETT first takes place at 10 GPa, $\rho(E_f)$ suddenly rises up, and this transition in turn perturbs the elastic constant. As Fig. 2 shows, C_{44} ceases its rising tendency at 13 GPa, which delays the occurrence of ETT at 10 GPa. One possible reason is that the ETT-induced energy shift cannot lead to a simultaneous effects because ETT occurs at 10 GPa. It is also speculated that an advanced treatment by taking into account the electron-phonon coupling or the strong correlation effects may lead to a better understanding between the two tendencies. For instance, in Ref. [43] it was reported that the DFT within the local density approximation and GGA will underestimate the critical value of ETT unveiled in experiments. It has been proved that the effects of ETT impact the elastic constant of Hf. However, for another 5d transition metal Os, C_{44} is hardly altered when it goes through the ETT. This can be explained by the retaining of the singularity in Os, but in Hf the singularity is weakened and eventually disappears. The distinct difference between Os and Hf is the number of valence electrons in d orbitals, which is relevant to the broadening of the band under pressure as well. Briefly, the singularity induced by ETT has a strong connection in enhancing C_{44}, but when it collapses, C_{44} shows a rapid attenuation.

Not only elastic constants but also the phonon anomalies are likely to be induced by ETT. As in Fig. 2, the inconsistent behavior between E_{2g} and C_{44} was observed. Actually, it was already suggested by McMahan [54–57] that the electronic topological changes can lead to phonon softening. The softening of E_{2g} remains from 0 to 13 GPa, and the E_{2g} mode experiences a jump once the ETT occurs. This follows the strengthened rising of C_{44} induced by ETT. When ETT takes place at 10 GPa, the curve of $\ln(c/a)/dP$ makes a turn from dropping down to rising, and after 17 GPa, $d\ln(c/a)/dP$ rises again. Note that both C_{44} and E_{2g} are consistently dropping off after 17 GPa. According to the behavior of $d\ln(c/a)/dP$, the ETT effectively reforms the regular pressure effects isotropically on solids between 10 and 17 GPa, results in the lattice and elastic anisotropy, and eventually leads to the anomalous behavior of C_{44} and E_{2g}.

V. CONCLUSIONS

In summary, the elastic modulus C_{44} in α Hf shows an increasing trend below 13 GPa. This is not in accordance with the consensual relation with the E_{2g} as observed in many other hcp transition metals. Our investigations reveal that it is due to the large anisotropy in α Hf under pressure. The anomaly found in lattice distortion can be well represented by $\ln(c/a)$, which can be measured and verified by experiment. The anisotropic distortion by compression is found along with the peculiar behavior of bands shift near the Fermi level. An in-plane ETT has been discovered along the A-H-L path. The strengthened rising of C_{44} is induced by the occurrence of ETT at 10 GPa, where the density of states shows an abrupt increase at the Fermi level. The large enhancement of the singularity from ETT promotes the rising of C_{44} around 13 GPa, and the diminishing of the singularity after ETT causes a softening above 17 GPa. The anisotropic distortion and the ETT under pressure govern the behavior of E_{2g}. Above the ETT critical pressure as well as the seeming delay of responses of C_{44} and E_{2g}, i.e., 17 GPa, the in-plane lattice is monotonically softening. Last but not least, the study establishes the relation between ETT, lattice anisotropy, and the anomalous behavior of C_{44} and E_{2g}, which therefore enriches the knowledge of high-pressure physics of transition metals.

ACKNOWLEDGMENTS

We would like to acknowledge Swedish Research Council (V.R.) for financial support, and HPC2N (High Performance

Computing Center North, Umeå, Sweden) and NSC (National Computer Center, Linköping, Sweden) in Sweden for the computational power. Weiwei Sun acknowledges the financial support from CSC scholarship leading to his doctoral study. The Fruitful discussion with Dr. Manuel Richter at IFW Dresden is also acknowledged.

[1] C. Leyens and M. Peters, *Titanium and Titanium Alloys: Fundamentals and Applications* (Wiley, New York, 2003).
[2] J. H. Schemel, *ASTM Manual on Zirconium and Hafnium* (ASTM International, Philadelphia, 1977), pp. 1–5.
[3] J. B. Hedrick, United States Geological Survey, retrieved (2008-09-10).
[4] D. Spink, Ind. Eng. Chem. **53**(2), 97 (1961).
[5] I. O. Bashkin, M. V. Nefedova, V. G. Tissen, and E. G. Ponyatovsky, JETP Lett. **80**, 655 (2004).
[6] H. Xia, G. Parthasarathy, H. Luo, Y. K. Vohra, and A. L. Ruoff, Phys. Rev. B **42**, 6736 (1990).
[7] E. A. Metzbower, Phys. Status Solidi B **25**, 403 (1968).
[8] J. C. Upadhyaya, D. K. Sharma, D. Prakash, and S. C. Upadhyaya, Can. J. Phys. **72**, 61 (1994).
[9] D. Antonangeli, M. Krisch, G. Fiquet, D. L. Farber, C. M. Aracne, J. Badro, F. Occelli, and H. Requardt, Phys. Rev. Lett. **93**, 215505 (2004).
[10] W. L. Mao *et al.*, J. Geophys. Res. **113**, B09213 (2008).
[11] C.-S. Zha, H. K. Mao, and R. J. Hemley, Proc. Natl. Acad. Sci. USA **97**, 13494 (2000).
[12] H. Olijnyk and A. P. Jephcoat, Solid State Commun. **115**, 335 (2000).
[13] H. Olijnyk and A. P. Jephcoat, Phys. Rev. B **56**, 10751 (1997).
[14] Y. K. Vohra and P. T. Spencer, Phys. Rev. Lett. **86**, 3068 (2001).
[15] H. Xia, S. J. Duclos, A. L. Ruoff, and Y. K. Vohra, Phys. Rev. Lett. **64**, 204 (1990).
[16] G. Jomard, L. Magaud, and A. Pasturel, Philos. Mag. B **77**, 67 (1998).
[17] Y. Hao, J. Zhu, L. Zhang, H. Ren, and J. Qu, Philos. Mag. Lett. **91**, 61 (2011).
[18] R. Ahuja, J. M. Wills, B. Johansson, and O. Eriksson, Phys. Rev. B **48**, 16269 (1993).
[19] www.ihed.ras.ru/elbrus12/program/restore.php?id=776
[20] C. Stassis, D. Arch, O. D. McMasters, and B. N. Harmon, Phys. Rev. B **24**, 730 (1981).
[21] I. M. Lifshitz, Sov. Phys. JETP **11**, 1130 (1960).
[22] G. Kresse and J. Hafner, Phys. Rev. B **48**, 13115 (1993).
[23] G. Kresse and J. Hafner, Phys. Rev. B **49**, 14251 (1994).
[24] K. Koepernik and H. Eschrig, Phys. Rev. B **59**, 1743 (1999).
[25] D. I. Khomskii, *Transition Metal Compounds* (Cambridge University Press, Cambridge, 2014).
[26] See Supplemental Material at http://link.aps.org/supplemental/10.1103/PhysRevB.95.115130 for brief description of material.
[27] Y. Le Page and P. Saxe, Phys. Rev. B **65**, 104104 (2002).
[28] X. Wu, D. Vanderbilt, and D. R. Hamann, Phys. Rev. B **72**, 035105 (2005).
[29] D. Alfè, Comput. Phys. Commun. **180**, 2622 (2009).
[30] J. P. Perdew and Y. Wang, Phys. Rev. B **45**, 13244 (1992).
[31] J. P. Perdew, K. Burke, and M. Ernzerhof, Phys. Rev. Lett. **77**, 3865 (1996).
[32] M. Methfessel and A. T. Paxton, Phys. Rev. B **40**, 3616 (1989).
[33] F. Birch, Phys. Rev. **71**, 809 (1947).
[34] F. D. Murnaghan, Am. J. Math. **59**, 235 (1937).
[35] F. D. Murnaghan, Proc. Natl. Acad. Sci. USA **30**, 244 (1944).
[36] A. Togo, F. Oba, and I. Tanaka, Phys. Rev. B **78**, 134106 (2008).
[37] H. Olijnyk and A. P. Jephcoat, J. Phys.: Condens. Matter **12**, 10423 (2000).
[38] T. Kenichi, Phys. Rev. B **56**, 5170 (1997).
[39] E. S. Fisher and L. C. R. Alfred, Trans. Metall. Soc. AIME **242**, 1575 (1968).
[40] K. Glazyrin *et al.*, Phys. Rev. Lett. **110**, 117206 (2013).
[41] Y. Kvashnin, W. Sun, I. D. Marco, and O. Eriksson, Phys. Rev. B **92**, 134422 (2015).
[42] L. Fast, R. Ahuja, Lars Nordström, J. M. Wills, B. Johansson, and O. Eriksson, Phys. Rev. Lett. **79**, 2301 (1997).
[43] L. Dubrovinsky *et al.*, Nature (London) **525**, 226 (2015).
[44] D. L. Novikov, A. J. Freeman, N. E. Christensen, A. Svane, and C. O. Rodriguez, Phys. Rev. B **56**, 7206 (1997).
[45] D. G. Pettifor, *Bonding and Structure of Molecules and Solids* (Clarendon, Oxford, 1995), pp. 182–191.
[46] H. L. Skriver, Phys. Rev. B **31**, 1909 (1985).
[47] J. S. Gyanchandani, S. C. Gupta, S. K. Sikka, and R. Chidambaram, J. Phys.: Condens. Matter **2**, 6457 (1990).
[48] T. Meissner S. K Goh, J. Haase, M. Richter, K. Koepernik and H. Eschrig, J. Phys.: Condens. Matter **26**, 015501 (2014).
[49] F. Bassani and G. P. Parravicini, *Electronic States and Optical Transitions in Solids* (Pergamon Press, New York, 1975).
[50] M. Ross and D. A. Young, Annu. Rev. Phys. Chem. **44**, 61 (1993).
[51] J, C. Duthie and D. Q. Pettifor, Phys. Rev. Lett. **38**, 564 (1977).
[52] J. A. Moriarty and A. K. McMahan, Phys. Rev. Lett. **48**, 809 (1982).
[53] M. I. Katsnelson, I. I. Naumov, and A. V. Trefilov, Phase Transitions **49**, 143 (1994).
[54] A. K. McMahan, Physica B+C **139-140**, 31 (1986).
[55] K. K. Pandey, J. Gyanchandani, M. Somayazulu, G. K. Dey, S. M. Sharma1, and S. K. Sikka, J. Appl. Phys. **115**, 233513 (2014).
[56] R. Hrubiak, V. Drozd, A. Karbasi, and S. K. Saxena, J. Appl. Phys. **111**, 112612 (2012).
[57] D. Koudela, M. Richter, A. Möbius, K. Koepernik, and H. Eschrig, Phys. Rev. B **74**, 214103 (2006).